DESIGN, CONSTRUCTION AND SIMULATION OF A UNIFORM MAGNETIC FIELD GENERATOR WITH STEEL NUCLEUS TO DEFLECT COSMIC RAYS

Karla Natalia Herrera Guzmán

University of Guanajuato, Department of Physics

herreragk2012@licifug.ugto.mx

Raúl Alejandro Gutiérrez Sánchez

University of Guanajuato, Department of Physics

gutierrezsr2012@licifug.ugto.mx

Jorge Luis Arceo Miquel

University of Guanajuato, Department of Physics

miquel@fisica.ugto.mx

Julián Félix

University of Guanajuato, Department of Physics

felix@fisica.ugto.mx

Resumen

La trayectoria de una partícula puede ser determinada midiendo algunos puntos por los que ha pasado. Esto se aplica a cualquier tipo de partículas, incluyendo rayos cósmicos. En este se presenta la construcción de un generador de campo magnético uniforme, dentro del cual se colocará un arreglo de detectores para medir las trayectorias de los rayos cósmcios. Presentamos detalles del diseño, construcción, calibración y algunos resultados preliminaries.

Palabras Claves: Bobinas, partícula relativista, rayos cósmicos, simulación.

Abstract

A particle's trajectory can be determined measuring some points where it has passed. This is applied to all kind of particles, including cosmic rays. In this paper

we present the construction of a uniform magnetic field generator. Inside it, an arrangement of cosmic ray detectors will be placed in order to measure cosmic ray trajectories. We present details of the design, construction, calibration and some preliminary physical results.

Keywords**:** *Cosmic rays, helmholtz coils, relativistic particle, simulation.*

1. Introduction

The cosmic rays are particles coming from outer space and they can be charged or neutral particles (charged cosmic rays at sea level are mostly muons). They were discovered in 1912 by Victor Hess. Since then, a lot of cosmic rays detectors have been built to study the universe. There are two types of cosmic rays: primary and secondary. The primary cosmic rays are generated by astrophysical sources such as supernovae, stars, pulsars, etc. The secondary cosmic rays are generated by collision of primary cosmic rays with interstellar gas, this means that earth atmosphere is a source of secondary cosmic rays [PDG, 2015].

The Cerenkov radiation is produced when a charged particle travels faster than light in a medium (radiator) [Mark, 2017], this radiation can be detected by photomultipliers. There are several types of cosmic ray detectors using Cerenkov radiation [Butslov, 1963], [Aseev, 1992], but most of them are based on transparent materials. New radiator materials could allow us to explore different energetic regions of detection and particles. Cosmic ray detectors usually are made of gases and liquids, among other transparent materials. The aim of this work is to know if Cherenkov radiation is produced in a material like aluminum, if so, it must be detectable. A uniform magnetic field deflects the charged particles trajectories, thus it is possible to use it with a particle detector. The objective is to detect the change in the direction of the cosmic rays and determine their energy, momentum, identity and trajectories. To achieve this, it is necessary to build a base to place an array of detectors inside the magnetic field generator. It is necessary that neither the detector's material nor the base's material distort the magnetic field. In this case we built the system for an arrangement of detectors of 8x8x8 in which consists of 32 Aluminum bars (1x2x8 in).

2. Methods

Analytic Description

Cosmic rays are very energetic, therefore it is considered a relativistic calculation about how they are deflected in a magnetic field. Starting with the Lorentz's principle [Serway, 2005] with no electric field

$$\vec{F}_{electromagnetic} = q\vec{v}x\vec{B},$$

Where q is the electric charge of the particle, $\vec{v}$ its velocity and $\vec{B}$ the magnetic field. Using the second Newton's principle with the relativistic correction, equation 1.

$$\frac{d\vec{p}}{dt} = q\vec{v}x\vec{B}, \tag{1}$$

Where $p = \gamma mv$ is the relativistic momentum ($v = \sqrt{\vec{v}\cdot\vec{v}}$).

Due to that a charged particle moving inside a uniform magnetic field follows a uniform circular motion (which implies that v is constant), γ is a constant. Because of this, and that $\vec{B} = (0, B, 0)$ and $\vec{v} = (v_x, 0, v_z)$, (1) is reduced to the following equations 2.

$$\begin{aligned} \gamma m\frac{dv_x}{dt} &= -qBv_z, \\ \gamma m\frac{dv_z}{dt} &= qBv_x, \end{aligned} \tag{2}$$

Defining $\alpha = \frac{\gamma m}{qB}$ and solving equation 2 we found equations 3 y 4.

$$x = \alpha\left[Asen\left(\frac{t}{\alpha}\right) - Bcos\left(\frac{t}{\alpha}\right)\right] + K \tag{3a}$$

$$z = -\alpha\left[Acos\left(\frac{t}{\alpha}\right) + Bsen\left(\frac{t}{\alpha}\right)\right] + C \tag{3b}$$

$$v_x = Acos\left(\frac{t}{\alpha}\right) + Bsen\left(\frac{t}{\alpha}\right) \tag{4a}$$

$$v_z = Asen\left(\frac{t}{\alpha}\right) - Bcos\left(\frac{t}{\alpha}\right) \tag{4b}$$

Applying the initial conditions $x = 0,\ z = z_0$ and $v_x = 0,\ v_z = v_{z0}$ in $t = 0$ to equations 3a, 3b, 4a and 4b, the solution is equations 5a and 5b.

$$x = \alpha\, v_{z0} cos\left(\frac{t}{\alpha}\right) - \alpha\, v_{z0} \tag{5a}$$

$$z = \alpha\, v_{z0} sen\left(\frac{t}{\alpha}\right) + z_0. \tag{5b}$$

The equations 5a and 5b have to be solved to find the maximum and minimum incidence speed in which the incident particle is going to be deflected in the desired way to find the lower and upper bounds for the energy. In order to solve this equations it is necessary to give the B, m, q y z_0 values, those are the magnetic field generated by the coils, the muon mass, the muon charge and the point in which the particle enters in the magnetic field.

Design

The prototype design consists in a pair of Helmholtz coils with 210 turns each and a ferric nucleus. Both coils are joined by steel bars to close the magnetic field. An aluminum base, which will be used to place detectors inside the magnetic field, was designed too. Figure 1 shows the design of the coils and the Aluminum base (drawn in SketchUp).

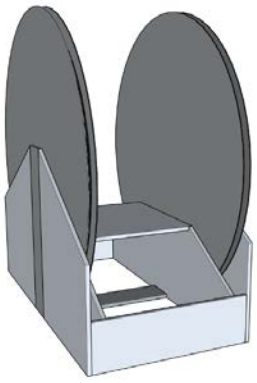

Figure 1 System perspective view.

In addition, the ferric pieces that makes the coils' reels, as well as the pieces that close the magnetic field, are made of ferric sheets to reduce possible eddy currents. The dimensions of the pieces in the design are shown in table 1. The shape and dimensions of some pieces are shown in figure 2.

Table 1 Pieces of the coil's reels and Aluminum base.

PIECES	MATERIAL	SIZE (cm)
4	Aluminum	Figure 4.1
2	Aluminum	Figure 4.2
2	Steel	27.22 x 5.00 x 0.40
1	Steel	23.72 x 5.00 x 0.40
1	Aluminum	20.32 x 20.32 x 0.40
2	Aluminum	23.72 x 10.00 x 0.40
PIECES	**MATERIAL**	**DIAMETER (cm)**
2	Steel	47.04
10	Steel	43.04

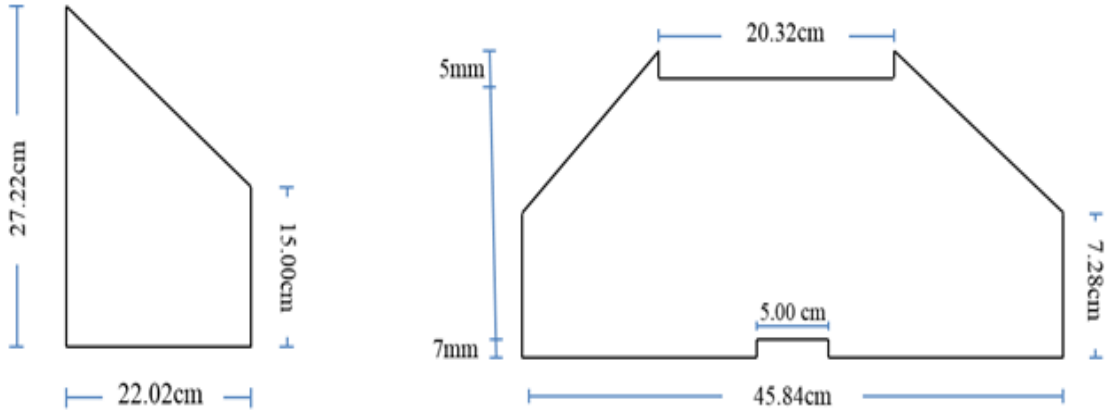

Figure 2 Dimensions and shape of two pieces of the Aluminum base.

All pieces in the design are joined together with nuts, bolts and Aluminum angles. Steel bolts are used to join steel pieces together and Aluminum bolts to join all Aluminum pieces.

This prototype is supposed to hold everything, including the electronic cards. Thus, a few Aluminum plates must be added. Those extra Aluminum plates are shown in figure 3. This figure also shows the way the 32 Aluminum bars will be placed inside the coils. Number 1 is an Aluminum plate needed to hold the connection strips (white rectangular prisms) needed to supply the voltage to the discriminator cards (dark green plates). Number 2 is an Aluminum angle that will be used to keep the photodiode cards (green plates) in its place (the latter ones will be screwed to the first one). Number 3 is an Aluminum plate and an Aluminum "C" that will support the discriminator cards outside the magnetic field.

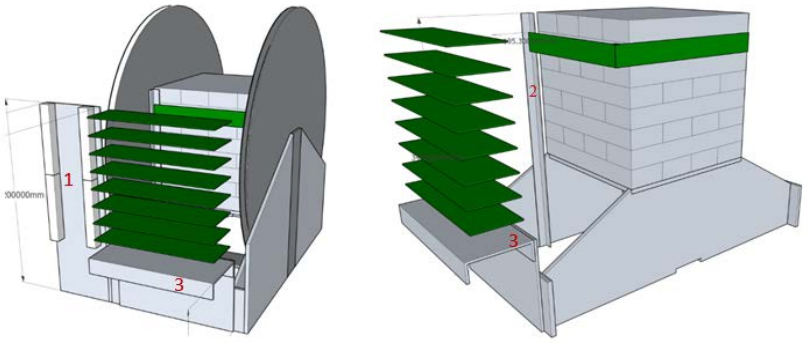

Figure 3 Design with aluminum pieces added to hold all electronic components.

Construction

All pieces in table 1 were cut with water jet. The steel pieces (Carbon steel A36) were cut from a steel sheet 18 AWG (0.91 mm) and the Aluminum pieces from a 5 mm thick aluminum plate.

Base Construction

The Aluminum angles and pieces were drilled. As the Aluminum bolts were too long to press the aluminum pieces together, we had to make washers. These washers were made with 5 mm thick black rubber. The washers used to fix the Aluminum square on top of the base, due to the limited space, are pre-made washers 1.2 mm thick.

Coils' Reels Construction

The steel laminas were glued together with JB Weld to form bars. The result was two bars of 27.5 x 5.0 x 0.6 cm and one of 23.4 x 5.0 x 0.6 cm (for future references this pieces are called L and K pieces respectively). The discs were perforated with 5 holes of 1/2 inch diameter. With the drilled discs were made 2 reels, each one containing two 23.4 cm radio discs and eleven 21.4 cm radio discs. The discs were glued together by the perimeter.

Assembly and Winding

The steel reels were winded with 210 turns each with 19 AWG wire. In the turn 120 it was necessary to put insulating tape to level them. After finishing the

winding, Qualtex Silicone was used in the top of the reels to protect the coils. L and K pieces are screwed together, so the necessary threaded holes were made. Finally, the reels were painted red color and the L and K pieces matte black color.

Coils' Electric Connection

To switch the magnetic field direction produced by the coils, it was used a two pole two throw switch, female banana connectors and connector strips. The components were connected with 5 mm red and black wire. The magnet wire of the coils was protected using thermofit.

Magnetic Field Mapping System

In order to map the magnetic field, a MakeBlock XY Plotter [MakeBlock, 2017] was adapted. A graduated (in millimeters) acrylic tube was used instead of a pencil. Inside the acrylic tube, a Vernier MG BTA gaussmeter [Vernier, 2017] was placed. With this modification was possible to map the magnetic field in a volume of 20.00±0.05 x 19.00 ±0.05 x 20.0 ±0.1 cm in x, y, z directions respectively. Figure 4 shows the measurement system on the prototype. Figure 5 shows the details of the measurements. In figure 5a the measurement system maps flat surfaces from left to right and to the electric connection "c", starting from the point in the red circumference. Figure 5b shows that the surfaces are mapped from the bottom to the top surface with a distance between them of d = 1 cm. Each surface is mapped in 20 lines from left to right; each line is made of 19 points. The mapped volume consists of 20 flat surfaces 1 cm apart.

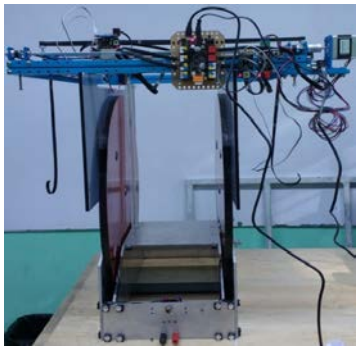

Figure 4 Measurement system on the prototype.

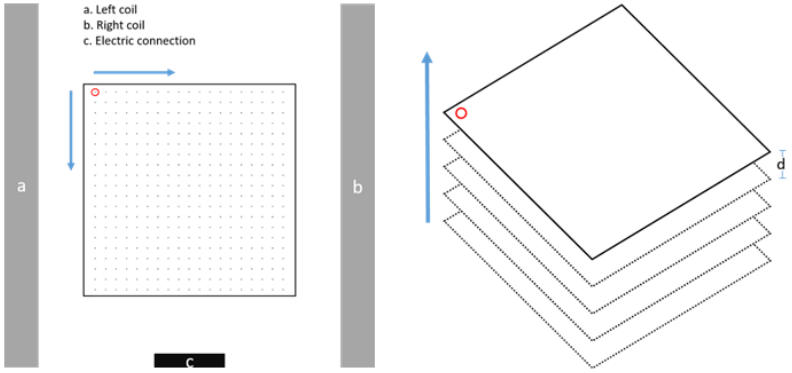

Figure 5 Scheme of the magnetic field mapping.

When the sensor in z direction is moved, it is possible that it got bend. Due to that this is a one direction magnetic field sensor, it is necessary to move it until it's parallel to the reels.

3. Results

Simulation

In order to have a prediction of the magnetic field that is generated by the coils, a model with real dimensions was sketched in Poisson Superfish [Poisson, 2017]. The resulting magnetic field is shown in table 2 when the current passing through the wire is between 1 and 20 amperes (the magnetic field magnitude at the center of the coils' axis). Figure 6 shows the generated graph by Poisson Superfish.

Table 2 Magnetic field magnitude obtained with Poisson Superfish, The relative μ value for the material of the reels is μ=250.

Current (A)	**2**	**4**	**8**	**10**	**12**	**14**	**16**	**18**	**20**
Magnetic Field (mT)	2.9	5.9	11.8	14.7	17.7	20.6	23.6	26.5	29.4

Magnetic Field Measurements and Prediction of the Equations (no core).

The predicted values were obtained by solving the Helmholtz coils equations and considering the middle point between coils on their common axis as origin. The resulting equation 6.

$$B = \frac{8 \cdot \mu_0 \cdot I \cdot N}{5 \cdot \sqrt{5} \cdot a}, \tag{6}$$

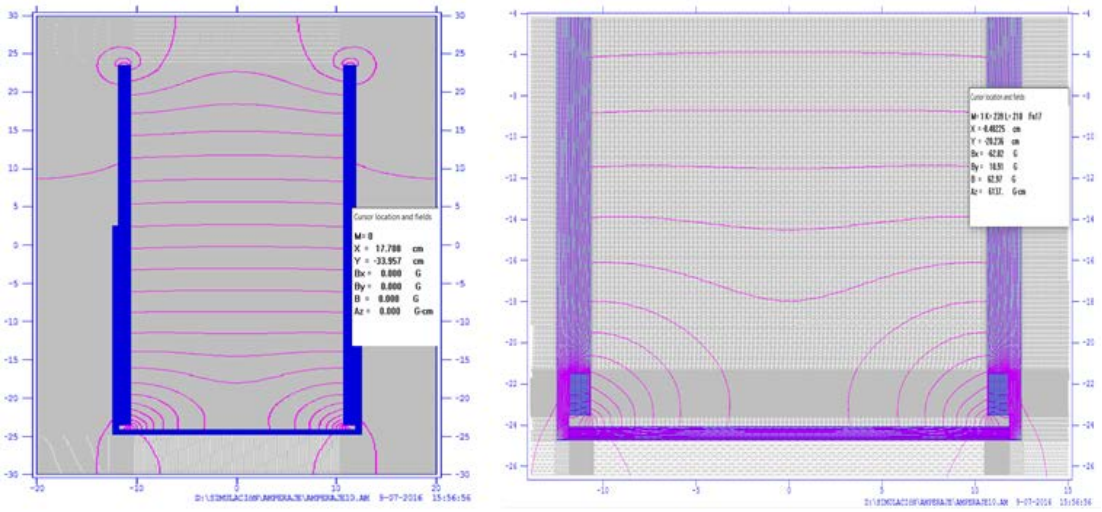

Figure 6 Magnetic field model.

where μ_0 is the vacuum permeability, I the electric current passing through the wire, N the number of turns, and a the radius of coils [Milford, 1995].

In order to obtain the multiplicative factor A that adjusts the simulation to the measurement (the factor that multiplies the measurements so they get as close to the simulation as possible), we start with the method of least squares [Steven, 2017].

$$\chi^2 = \sum_{i=1}^{n} \frac{(B_{simi} - AB_{mi})^2}{(\Delta B_{mi})^2}, \tag{7}$$

Where B_{simi} is the obtained magnetic field value by the simulation, B_{mi} is the measured magnetic field value. Equating the first derivative of equation 7 to zero and considering an error of 5% ($\Delta B_{mi} = 0.05 \cdot B_{mi}$), A and ΔA are obtained equations 8 y 9.

$$A = \sum_{i=1}^{n} \frac{B_{simi}}{n \cdot B_{mi}}, \tag{8}$$

$$\Delta A = \sqrt{\sum_{j=1}^{n} \frac{{B_{simi}}^2 \cdot 0.0025}{n^2 \cdot {B_{mi}}^2}}. \tag{9}$$

The multiplying factor that makes the simulation values closer to the measurements (C) is related with A as equation 10.

$$C = \frac{1}{A} \cdot \text{with} \cdot \Delta C = \frac{1}{A^2} \cdot \Delta A. \quad (10)$$

To pass from the predictions factor to measurements factor, the following changes have to be made $B_{simi} = B_{mi}$ and $B_{mi} = B_{pi}$, with the subscript pi denoting the prediction values. Table 3 shows ten measurement points (n=10) with their respective electric current values. In these 10 points, A and C were measured for simulation (subscript s) and prediction (subscript p) cases, these results are given in table 4. Figure 7 shows measurement, simulation and prediction results.

Table 3 Electric current values.

n	1	2	3	4	5	6	7	8	9	10
I (A)	0.5	1.0	1.5	2.0	2.5	3.0	3.5	4.0	4.5	5.0

Table 4 Multiplying factors.

	A_s	C_s	A_p	C_p
Value	1.28	0.75	1.38	0.72
Error	0.05	0.03	0.05	0.03

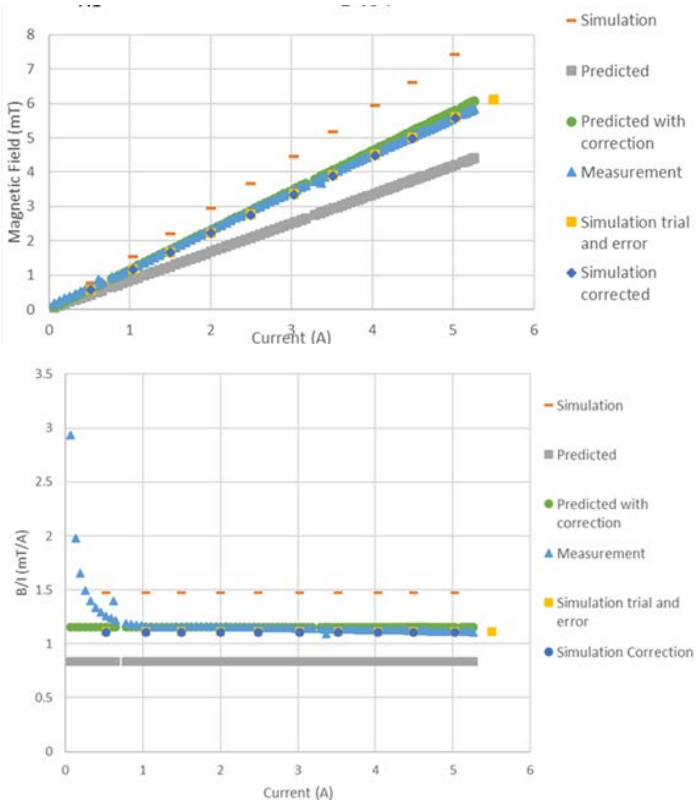

Figure 7 Measurement, simulation and prediction results.

The measurements in figure 7 were made with a VGA AlphaLab sensor, this measurements are consistent with the Vernier sensor. Yellow points are obtained by modifying the μ value in the simulation by trial and error until we found a value of B approximated to the measurements, the μ value obtained is μ =120.05. The values indicated by “Simulation Correction” (dark blue) are the values obtained by multiplying $\mathbf{C_s}$ with the original simulation values to make them fit with the measurement values. The green values are obtained in the same way that the dark blue ones, but this time multiplying the predicted values (gray) with $\mathbf{A_p}$ to fit the predicted values to the measurements.

Relativistic Particle Kinematics.

The values needed to solve equations 5a and 5b are:

$B = 29.4429\text{mT}$ (obtained from Poisson Superfish for a 20 Amperes current).

$$m = 1.08838x10^{-28}\,\text{kg}$$

$$q = \pm 1.0602x10^{-19}\,\text{C}$$

$$z_0 = 23.52\,\text{cm}$$

Defining $\beta = \frac{m}{qB}$, the equations 11.

$$x = \frac{\pm\beta xc}{\sqrt{c^2 - {v_{z0}}^2}} \cdot v_{z0}\left[cos\left(\frac{\sqrt{c^2 - {v_{z0}}^2}}{\beta xc} \cdot t\right) \mp 1\right],$$
$$z = \frac{\pm\beta xc}{\sqrt{c^2 - {v_{z0}}^2}} \cdot v_{z0}\left[sen\left(\frac{\sqrt{c^2 - {v_{z0}}^2}}{\beta xc} \cdot t\right) \mp 0.2352\right]. \quad (11)$$

To find the incidence speed of the particle we must give conditions to the energy bounds, see figure 8 which are:

Upper bound; case in which the particle leaves the array of detectors without a detectable deflection (green, the width of one detector is 5.08 cm):

$$x = \pm 0.0508\text{m},\ \ z = -0.1016\text{m}.$$

Lower bound; case in which the particle leaves the array of detectors before crossing its half (red):

$$x = \pm 0.1016\text{m}, \quad z = 0.0254\text{m}$$

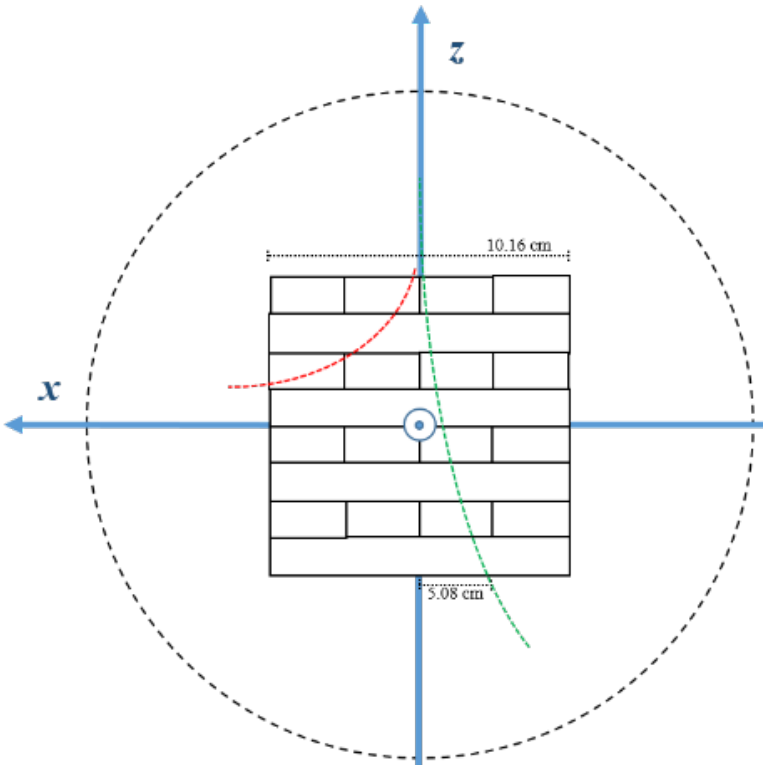

Figure 8 Energy bounds. In red, the trajectory of a particle passing through the lower bound; in green, the one which goes through the upper bound.

As equations 12 are nonlinear equations, it was necessary to use an internet platform called “WolframAlpha” to solve them. The results obtained are:

Lower Bound: $v_{z0} = -6.7\text{x}10^{6}\,\frac{\text{m}}{\text{s}}.\ t = 3.6x10^{-8}\text{s}.$

Upper bound: $v_{z0} = -2.8\text{x}10^{7}\,\frac{\text{m}}{\text{s}}.\ t = 1.2x10^{-9}\text{s}.$

The energy bounds according to these velocities are:

$$E_{max} = 106.3\text{MeV}, E_{min} = 105.9\text{MeV}.$$

Automated Magnetic Field Map

When the coils were powered with 100 V, the power supply was giving about 6.6 A, but they started to warm up. This made the 6.6 A to decrease rapidly. The current output stabilized about 1.5 hours later, having around 4.7 A and an

approximated temperature of 78 °C. It is at this point where the magnetic field measurements takes place. It is necessary to point out that the rising of the temperature deforms the acrylic tube. This makes that the measurements in the vicinity of the reels are made with a deformed acrylic tube. The acrylic tube is separated from the aluminum square 1.52±0.01 mm (before deformation). Table 5 shows the initial and final current and temperatures in which the measurements took place for every plane.

Table 1 Values of current and temperature between each plane was mapped.

Plane number	I_i (A)	I_f (A)	T_i (°C)	T_f (°C)
0	4.767	4.695	72.5	77.0
1	4.675	4.669	78.8	78.8
2	4.668	4.665	79.5	79.4
3	4.665	4.660	79.4	79.7
4	4.661	4.660	79.8	80.0
5	4.760	4.690	71.6	77.3
6	4.690	4.680	77.3	77.5
7	4.680	4.666	77.7	78.8
8	4.667	4.662	79.1	79.7
9	4.662	4.657	79.7	80.2
10	4.657	4.657	80.3	80.2
11	4.658	4.659	80.4	80.2
12	4.807	4.713	68.4	75.5
13	4.712	4.686	75.7	76.8
14	4.686	4.674	76.8	77.5
15	4.674	4.666	78.2	78.6
16	4.666	4.665	78.7	78.9
17	4.665	4.663	78.9	79.1
18	4.663	4.665	78.7	78.8
19	4.665	4.673	78.4	78.4
20	4.704	4.690	77.0	78.5

Figure 9 shows the graphs of the initial, final and central mapped plane, the rest of the planes were omitted because this planes are enough to realize the way the magnetic field changes with the z position.

In table 6 it is shown the maximum and minimum of each plane and its proportion. The last row shows the maximum variation of the entire map (21 planes) taking the global maximum and minimum. Figure 10 shows the graphs of the values in table 6.

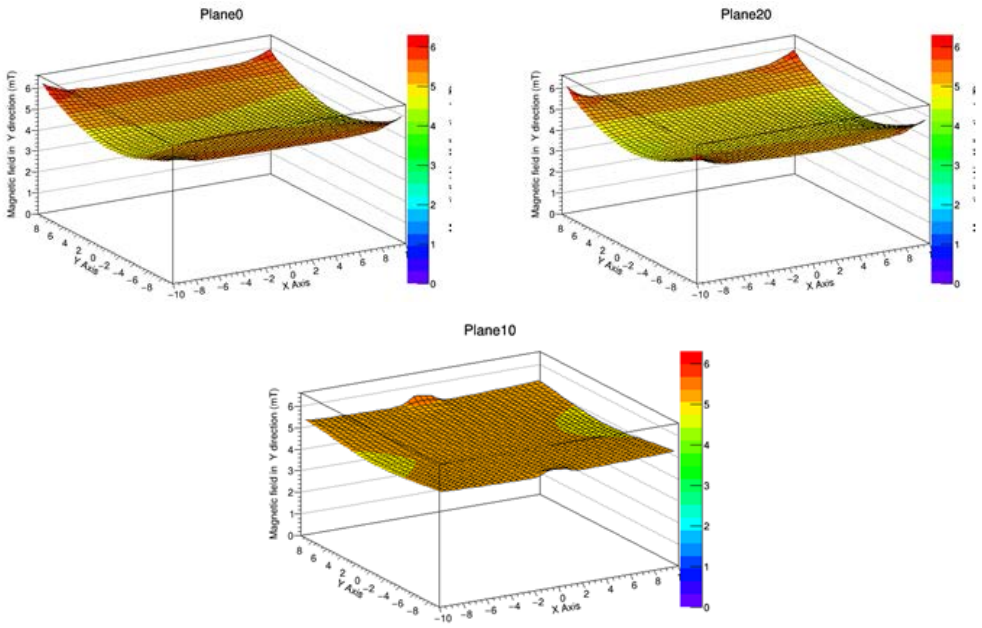

Figure 2 Graphs of each one of some mapped planes.

Table 2 Maximum and minimum values of each plane and its percent variation.

Plane	Max (mT)	Min (mT)	Variation
0	6.3	4.7	1.4
1	5.7	4.7	1.2
2	5.6	4.7	1.2
3	5.5	4.8	1.2
4	5.5	4.8	1.1
5	5.6	4.9	1.1
6	5.5	4.9	1.1
7	5.5	4.9	1.1
8	5.4	4.9	1.1
9	5.8	4.9	1.2
10	5.7	4.9	1.2
11	5.4	4.9	1.1
12	5.5	4.9	1.1
13	5.4	4.9	1.1
14	5.4	4.8	1.1
15	5.3	4.7	1.1
16	5.3	4.6	1.1
17	5.3	4.6	1.2
18	5.7	4.6	1.2
19	6.3	4.5	1.4
20	6.3	4.4	1.4
Maximum variation	6.3	4.4	1.4

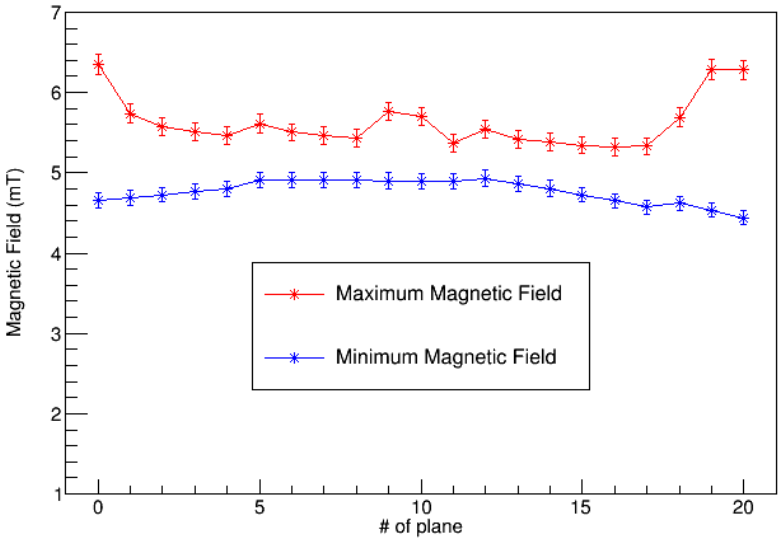

Figure 10 Maximum and minimum magnetic field values.

4. Discussion

This cosmic ray detector will have the unique characteristic that uses a metal as a radiator material for Cherenkov radiation. Some very preliminary tests have been done and we know we measure something in the aluminum bars, but we still have to do more tests to demonstrate that it is Cherenkov radiation. No other country is developing this kind of detectors. One of the advantages about using metals is that you do not have to isolate them of external radiation, they are easily mounted and the maintenance is much easier than for liquids and gases.

5. Conclusions

We have designed, constructed and characterized a device to create a uniform magnetic field. We have simulated the magnetic field as a function of electric current; we have predicted the magnetic field proportional to the applied electric current; we have measured the magnetic field as a function of the applied electric current.

The prediction and simulation results were adjusted to the results of the measurements by least square method and to the measurements to obtain the μ_r of the utilized material of the coils' core resulting A_p=μ_r=1.38 ±0.05*μ_0 (figure 7). This is a technique to measure the magnetic permeability of the coils' core.

Incident cosmic particles with energy between E_{max}=106.311 MeV and E_{min}=105.858 MeV must be detected by this spectrometer. Loss of energy from particles passing through the detectors is not considered.

Magnetic field percent variation decreases as the sensor approaches to the axis of the coils and increases as they move away from it. Also it is observed that this variation increases faster in the upper planes than in the lower planes.

6. Bibliography and References

[1] Mark Chen, Queen's University. Scintillation and Light Sensitive Detectors. http://neutron.physics.ucsb.edu/docs/scintillation_presentation_info.pdf, March 11, 2017.

[2] Aseev, E.G. Devitsin, A.A. Komar, V.A. Kozlov, Yu.I. Hovsepyan, S.Yu. Potashov, K.A. Sokolovsky, T.V. Uvarova, Nuclear Instruments and Methods in Physics Research Section A: Accelerators, Spectrometers, Detectors and Associated Equipment 317 pp. 143-147, 1992.

[3] Butslov M. M., Medvedev M. N., I V Chuvilo and M V Sheshuno, Nuclear Instruments And Methods 20, pp. 263-266, 1963.

[4] Makeblock, website, http://learn.makeblock.com/xy-plotter-robot-kit/. August 11, 2017.

[5] PDG (Particle Data Group), http://pdg.lbl.gov/2011/reviews/rpp2011-rev-cosmic-rays.pdf, January 2017.

[6] Poisson Superfis: http://laacg.lanl.gov/laacg/services/download_ sf.phtml, August 11, 2017.

[7] Reitz J. R. y F. J. Milford, Fundations of Electromagnetic Theory (Massachusetts/Adison-Wesley) Capítulo 8, pp. 165-166, 1992.

[8] Serway R. A. y R J Beichner, Fisica para ciencias e ingenierías. Tomo II (Mexico/McGraw-Hill) Chapter 29, pp. 922, 2001.

[9] Steven J. Miller. The method of Least Squares 0. https://web.williams.edu/Mathematics/sjmiller/public_html/BrownClasses/54/handouts/MethodLeastSquares.pdf, August 11, 2017.

[10] Vernier, https://www.vernier.com/products/sensors/mg-bta/, January 2017.